K-edge near-edge x-ray-absorption fine structure of oxygen- and carbon-containing molecules in the gas phase

T. K. Sham
Department of Chemistry, The University of Western Ontario, London, Canada N6A 5B7

B. X. Yang*
Physics Department, University of British Columbia, Vancouver, British Columbia, Canada V6T 2A6

J. Kirz
Physics Department, State University of New York at Stony Brook, Stony Brook, New York 11794

J. S. Tse
Chemistry Division, National Research Council of Canada, Ottawa, Canada K1A 0R9
(Received 7 November 1988)

The carbon and oxygen *K*-edge near-edge x-ray absorption fine structures (NEXAFS) of a series of molecules, carbon monoxide (CO), carbon dioxide (CO_2), carbonyl sulfide (OCS), acetone [$(CH_3)_2CO$], ethanol (C_2H_5OH), diethylether [$(C_2H_5)_2O$], tetrahydrofuran (C_4H_8O), and *p*-dioxane ($C_4H_8O_2$) have been recorded in the gas phase in transmission, total-ion-yield, and luminescence-yield modes. The results are compared with previous measurements and theoretical predictions, and discussed generally on the basis of molecular structure and bonding. The the NEXAFS parameters are examined in terms of the electron-core-hole interaction, spatial characteristics of the final states, correlation with interatomic distance, and multiple-scattering phenomena.

I. INTRODUCTION

The rapidly increasing availability of synchrotron radiation has generated a great deal of interest in gas-phase inner-shell-excitation spectroscopies and related phenomena of low-*Z* (atomic number) elements in molecules. The current generation of electron storage rings and optical instruments can routinely provide high-flux monochromatic photons ($>10^9$ photons/sec mm^2 with good resolution) in the vuv and soft-x-ray regions (100–3000 eV) required for some gas-phase experiments. Thus a number of gas-phase soft-x-ray absorption and related experiments have been performed.[1–15] One of the main areas of interest is the dynamics of the core-level photoabsorption processes in the vicinity of an ionization threshold (near-edge region) and the extended energy regions above the threshold [extended x-ray-absorption fine structure (EXAFS) region].

The second-row elements are ideally suited for these studies because the *K* shells of these elements are the only atomic levels they possess as their *L* shells are in the valence region and are actively involved in bonding. Since these electrons are intimately involved in the decay of the core hole, the decay process itself and its products are sensitive to the chemical environment. The main objective of our studies is to investigate the influence of the chemical environment (molecular potential) on inner-shell photoabsorption and subsequent decay processes. Experimental investigations to achieve this goal have led to the development of a great variety of techniques[16] such as yield spectroscopies (total electron, partial electron, photoelectron, Auger electron, selected ion, fragmentation, fluorescence, and luminescence) and resonance spectroscopies (such as resonant Auger and resonant photoemission) as to be compared to the conventional absorption and photoionization techniques.

All the yield techniques for absorption-type measurements are based on the idea that within the framework of a single-particle process, all the yields are proportional to the number of photons absorbed (hence the absorption coefficient). This has been shown to be more or less the case in EXAFS experiments, although the correct EXAFS amplitude cannot always be obtained in yield measurements.[14–26] More dramatic differences are expected in the near-edge region among different yield techniques where several different excitation channels are accessible in molecules: (a) bound-to-bound (molecular-orbital) transition, (b) bound-to-bound (Rydberg) transition, (c) bound-to-quasibound (virtual-molecular-orbital or shape-resonance) transition, and (d) bound-to-continuum transitions (multiple-scattering-type photoelectron diffraction at low and intermediate energies) and each of these channels may decay differently depending on the electronic nature of the final state and the interaction between the electron and the core hole. Thus yield spectra based on detecting one specific kind of particle (within a specific energy range) would have varying degrees of sensitivity for these excitations. In EXAFS at high energies, however, the one-electron ionization channel usually dominates. In addition, single-particle processes are often accompanied by many-particle processes (such as shake-up and shake-off), sometimes with appreciable in-

tensity. It is reasonable to expect that the correlation of the yield with absorption in the near-edge x-ray-absorption fine structure (NEXAFS) region depends critically on the nature of the yield used in the measurement. For example, selected ion yield (fragmentation) and luminescence yield have been shown to be photon energy selective for some molecules in the NEXAFS region.[1,6,13,14]

Several aspects of photoabsorption are of concern in our studies. First, we are interested in the comparison of absorption measurements with photoionization and other yield measurements, particularly fragmentation, and luminescence yield. Second, we are interested in the dynamic process through which the energy of the photon absorbed by the molecule is redistributed via photoelectron emission and the decay of the core hole. Events such as Auger-electron emission, fluorescence, fragmentation of molecules, and luminescence are results of the decay of the core hole. Monitoring these events as a function of photon energy in turn will greatly facilitate the assignment of the absorption spectrum. Thus it can be expected that if all these partial yield (cross-section) events were measured concurrently with the conventional absorption measurement, detailed information concerning photoabsorption dynamics could be obtained. The ionization and luminescence measurements reported here are aimed towards this goal. Finally we want to study the chemical systematics of the NEXAFS of these molecules and in particular their molecule shape resonances.[27–31] The study of core-excited molecular shape resonances has attracted much attention lately in connection with their correlation with bond length in small molecules suggested by Hitchcock and co-workers[32,33] There has been a debate on the validity of such a correlation.[34–36] One of the problems in this controversy is the assignment of the shape resonance. Most of the data used in these studies so far are from electron energy loss spectroscopy (EELS) measurements[32] which have great sensitivity and resolution near the threshold but the sensitivity drops markedly (proportional to E^{-3}, E is the energy loss) at energies farther from the threshold. Therefore when a weak resonance is observed at 20 eV above the threshold in the EELS spectrum, its assignment to molecular shape resonance is sometimes justifiably challenged (shake-up would be the alternative assignment). We believe that NEXAFS absorption measurements using synchrotron radiation will complement the EELS data in this energy region. Thus absorption and yield measurements with synchrotron radiation to extended energies (including EXAFS) in combination with theory will greatly facilitate the understanding of the core-excited molecular shape resonances of small molecules.

It has been our continuing effort to study the K-edge photoabsorption of low-Z elements in molecules containing carbon and oxygen in the gas phase. What can be learned from the gas-phase experience will benefit the study of similar phenomena in condensed phase and on surfaces. In a recent study,[11] we reported the high-energy features (molecular EXAFS) above the oxygen K edge of a series of molecules containing carbon–oxygen bonds: CO, CO_2, OCS, $(CH_3)_2CO$, C_2H_5OH, $(C_2H_5)_2O$, C_4H_8O (tetrahydrofuran, THF), and $C_4H_8O_2$ (p-dioxane). We found that the single-particle, single-scattering theory with plane-wave approximation is inadequate in describing the EXAFS of these molecules with low-Z elements and short bonds. Chemical transferability has only limited success in closely related molecules. In this paper, we report the low-energy absorption features (NEXAFS region) of the same series of molecules at both the carbon and oxygen K edge.

This paper is arranged as follows: In Sec. II the experimental procedure and data analysis are described, following by the results and observations in Sec. III. The chemical systematics of the NEXAFS of these molecules are discussed in Sec. IV. The correlation of the shape resonance and the oscillatory features beyond the shape resonance at the carbon K edge with bond length are given in Sec. V. X-ray-absorption measurements with luminescence yields are discussed in Sec. VI. Summary and conclusions are given in Sec. VII.

II. EXPERIMENTAL PROCEDURE

The experiments were carried out at the U15 beam line of the National Synchrotron Light Source, Brookhaven National Laboratory. This beam line is equipped with a toroidal grating monochromator (TGM) with a 600-line/mm gold-coated grating. The measurements were made with a modified Samson-type ion chamber (Fig. 1) which has been described in detail elsewhere.[7,11–13] An ultrathin silicon nitride window (1300 Å thick) was used to separate the gas from the rest of the beam line. This allows us to carry out the experiments at relatively high pressure (0.1–1.0 Torr) which was essential for measurements with high signal-to-noise ratio without using multistage differential pumping. The length of the photon path in the sample gas was chosen to be 83.8 mm which enables us to use the thin-sample approximation at the lower end of the pressure range, i.e., $\exp(-\mu t) \approx 1-\mu t$, where μ is the linear absorption coefficient. The absorbed flux of photons can thus be expressed as $I_0\mu t$, where I_0 is the incoming flux, and the secondary yield spectra can be simply expressed as $I_0\mu t f(E)$, where $f(E)$ is the conversion factor of the yield. In general, $f(E)$ varies smoothly with the photon energy E far above the edge and the

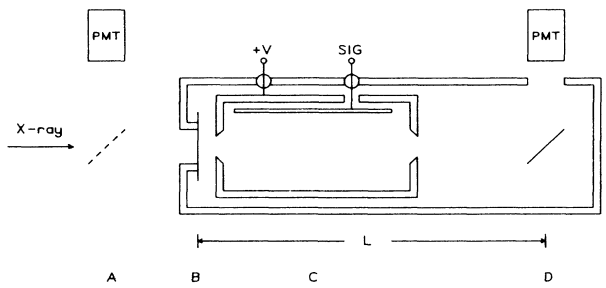

FIG. 1. Schematics of the experimental arrangement: A and D are the photon monitors, B is the silicon nitride window, and C is the ionization chamber.

yield is proportional to the absorption coefficient. Higher-order contribution of this monochromator is considerable especially in the energy region below 500 eV. The second-order radiation can be used to record the oxygen K-edge absorption spectrum which would appear at around 260 eV (together with the first-order spectrum of the C K edge). Fortunately, the molecules being studied have a small and smooth cross section (for the first-order radiation) in the energy range below the carbon K edge. Therefore, oxygen NEXAFS can be studied conveniently with second-order photons. This measurement provides not only more accurate energy calibration between oxygen and carbon K-edge features but also x rays with better resolution. Figure 2 illustrates the improvement in energy resolution of the acetone O K-edge spectrum using second-order radiation. In the second-order spectrum, the width of the O $1s$-to-π^* transition (2.5 eV) is 30% narrower and features unresolved in the first-order spectrum are revealed [resolution is 1.6 eV full width at half maximum (FWHM) at C K edge and 2.6 eV at O K edge]. We shall discuss further details in the following sections.

Both the incoming (I_0) and the transmitted (I) x-ray intensities were measured with phosphor detectors.[37] The spectral response of the phosphor (P31) does not contain any sharp features in the energy range of the experiment. However, its response is roughly linear with the photon energy, and hence the second-order spectrum is enhanced in the data shown here. It should also be noted that since the absorption of the window differs for the photons of different energies, spectral structures in the incoming x-ray beam will not be completely removed when the data are normalized using vacuum scans. Although we have developed a procedure to correct the artifact when the second-order radiation is weak,[11] strong intensities of higher orders in this experiment simply do not allow us to make such elaborate corrections. The as-recorded spectra presented here should be taken as semi-quantitative when spectral intensities are compared at different edges. Nevertheless, we believe that all the major features are real and reproducible.

Two photomultiplier tubes (PMT) were used to record the phosphoresence intensity of the flux monitors. A third PMT, mounted perpendicularly to the beam axis, was used to monitor the optical luminescence (signal denoted as I_l) induced by the photons in the sample gas. The ion current (signal denoted as I_i) and the PMT current were amplified by current amplifiers, digitized by voltage to frequency converters, and recorded by computer aided measurement and control (CAMAC) scalers interfaced with a PDP-11/23 computer.

Three modes of measurements, absorption, total ionization yield, and optical luminescence yield were simultaneously employed in recording the "absorption spectra" at both the oxygen and the carbon K edges. The transmission function of the window was measured by a spectral scan without sample gas in the chamber (vacuum scan), and was used to normalize all three kinds of spectra taken with the sample gases.[11] The data thus obtained are present as I_0/I, I_i/I_0, and I_i/I_0 in arbitrary units for absorption, ionization and luminescence cross sections, respectively, versus photon energy.

III. RESULTS AND GENERAL OBSERVATIONS

The oxygen and carbon K-edge NEXAFS of CO recorded in the three different modes are shown in Fig. 3.

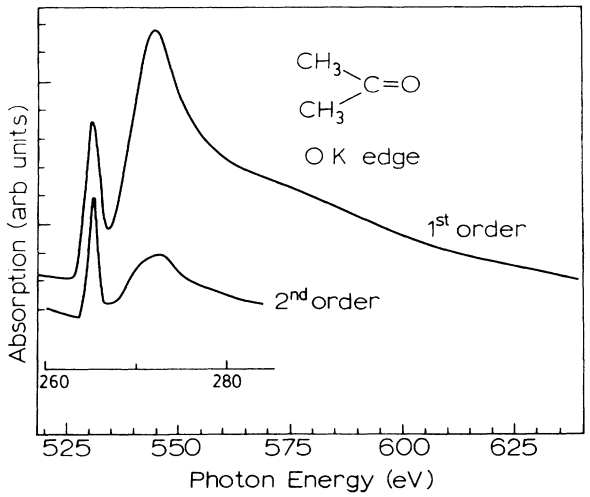

FIG. 2. Oxygen K-edge spectrum of acetone recorded with first- and second-order radiation.

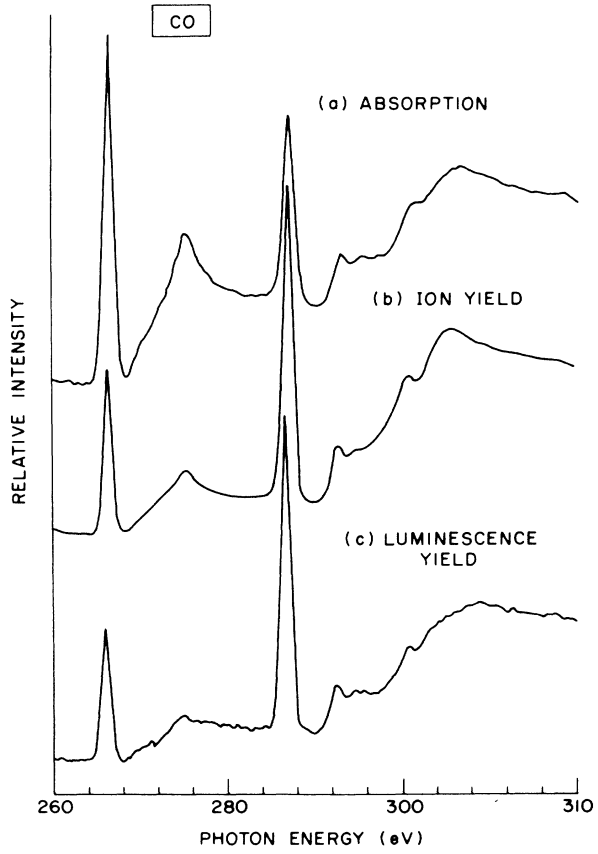

FIG. 3. Carbon and oxygen K-edge spectra of CO recorded with first- and second-order radiation, respectively.

Since second-order radiation was a significant part of the photon beam in these measurements, the oxygen K-edge spectrum appears at energies below the carbon K edge from 260 up to 285 eV (520 and 570 eV in second order) with appreciable intensity. Above 285 eV the oxygen feature is obscured by the intense carbon absorption. Fortunately, the oxygen absorption above this energy is weak relative to the NEXAFS structure of carbon and is slowly varying (Fig. 2).[11] At the C K edge, however, the second-order radiation not only contributes to the base line but also suppresses sharp absorption features (thickness effect[38]). The most noticeable difference among these spectra is the relative intensity of the edge jump of oxygen and carbon and the relative intensity of the resonances in the absorption spectrum [Fig. 3(a)] relative to those of the yield spectrum [Figs. 3(a) and 3(b)]. The relative enhancement of the O K-edge spectrum in Fig. 3(a) is the result of the more sensitive response of the transmitted flux detector (I) to second-order relative to the first-order radiation.[11,37] The general features are very similar in all the spectra except in the region above the threshold where the ion yield spectrum is always more intense. Hitchcock *et al.*[39] have recently addressed this situation extensively. Of the three techniques the ion yield always gives the best signal-to-noise ratio and these spectra are used for the identification of the absorption features and for comparison among different compounds.

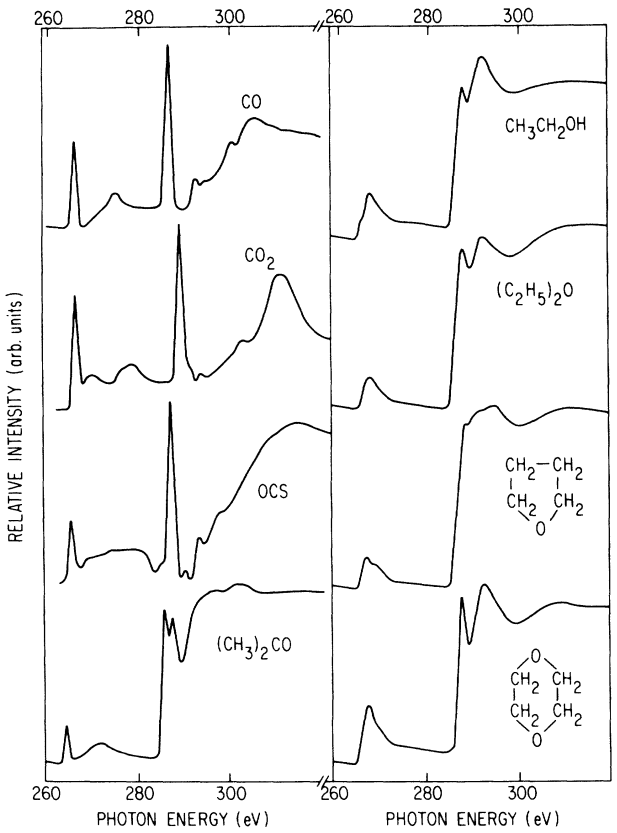

FIG. 4. Overall comparison of the O (second order) and C K-edge spectra of molecules reported in this study.

The carbon and oxygen K-edge spectra obtained in the ionization mode (total ion yield) for all the molecules studied are shown in Fig. 4 and the ion-yield and luminescence-yield spectra of linear polyatomic molecules CO_2 and OCS with unsaturated carbon-oxygen bonds are shown in Fig. 5. Both yield results are very similar except that in the region above the threshold, the luminescence intensity is weaker, similar to what is observed in the CO spectra. More drastic difference between the ion yield and the luminescence yield spectra is seen in molecules having saturated carbon-carbon and carbon-oxygen bonds. Some representative results are shown in Fig. 6 where the difference between the ion yield and the luminescence yield above the threshold is clearly noticeable.

The general appearance of the NEXAFS and their assignment are discussed below in some detail. To facilitate

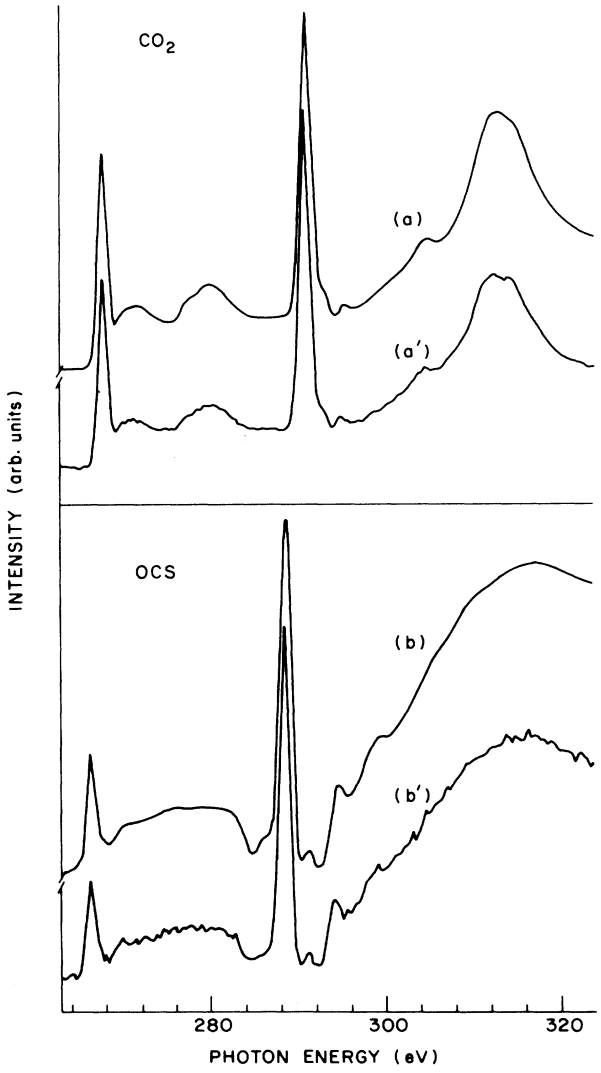

FIG. 5. Comparison of ionization-yield [(a) and (b)] with luminescence-yield spectra [(a') and (b')] for CO_2 and OCS, respectively.

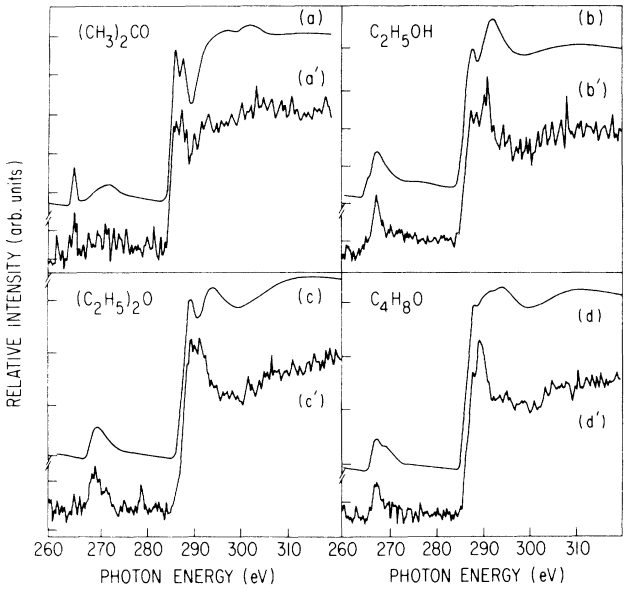

FIG. 6. Comparison of ionization yield [(*a*)–(*d*)] with luminescence yield spectra [(*a'*)–(*d'*)] for acetone and selected saturated molecules.

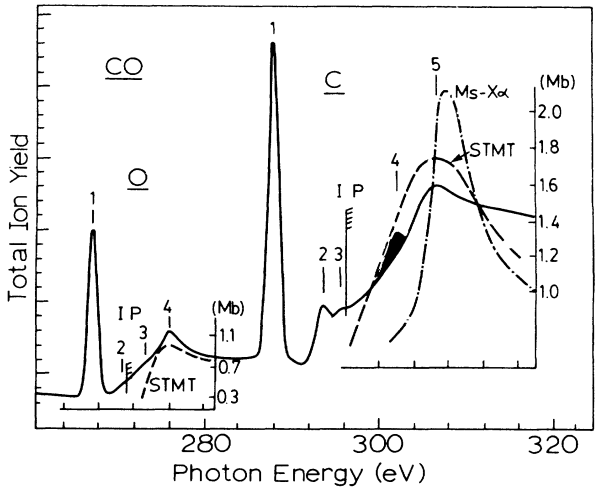

FIG. 7. Carbon and oxygen *K*-edge spectrum of CO scaled to absolute cross sections (oxygen edge was scaled according to the results of Ref. 11, the carbon value was scaled according to the atomic values of Ref. 77) and theoretical predictions (see Table I for assignments).

the discussion, the molecules are divided into three different groups: (a) linear molecules with unsaturated C—O bonds (CO, CO_2, OCS); (b) polyatomic molecule with a saturated C—C bond and an unsaturated C—O bond [$(CH_3)_2CO$, acetone]; and (c) polyatomic molecules with saturated C—C and C—O bonds [C_2H_5OH, ethanol; $(C_2H_5)_2O$, diethyl-ether, C_4H_8O, tetrahydrofuran, THF; and $C_4H_8O_2$, *p*-dioxane].

A. NEXAFS of linear molecules CO, CO_2, and OCS

The *K*-edge absorption spectra of these molecules have been studied by many research groups,[2,4,40–45] therefore detailed assignment to each absorption feature is not discussed here except in cases where previous measurements have not been reproducible or assignments are uncertain. Following a simple minimal-basis-set molecular-orbital approach (only 2*s* and 2*p* orbitals are considered) in which all the final states are viewed as molecular orbital with prominent π^* or σ^* character, we first assign the prominent features, then compare the data with more sophisticated calculations.[46–52] It should be noted that excitation and ionization in the vicinity of the threshold need not be explicitly distinguished by their energy positions relative to the ionization threshold and the absorption spectrum can be viewed as a convolution of the square of the transition matrix element with the density of unoccupied states of a selected symmetry in the vicinity of the absorbing atom.

The carbon and oxygen *K*-edge spectra for CO and CO_2 are shown in Figs. 7 and 8, respectively, together with previous theoretical predictions.[46–52] The peak positions and assignments are listed in Table I together with the EELS results of Wight and Brion[42] and x-ray-absorption results of Barrus *et al.*[43] It can be seen from Table I that the peak positions generally agree very well except that of the shape resonances which appear at higher energy in our data than in the EELS spectrum. We will return to this point in a later discussion. Let us neglect the shaded areas in Figs. 7 and 8 for the moment. It is evident from these figures that all of the spectra exhibit a sharp resonance ($1s$-π^*) below the ionization threshold and a broad resonance (σ^*) above the threshold except in CO_2 of which the O *K*-edge spectrum exhibits two resonances.

We first attempt to understand these prominent resonances on minimal-basis-set molecular-orbital (MO) con-

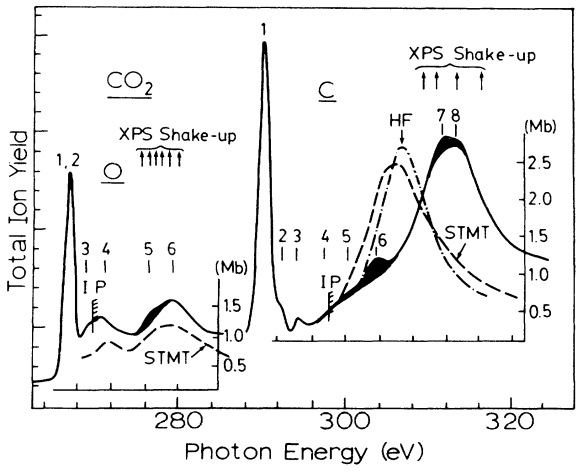

FIG. 8. Carbon and oxygen *K*-edge spectrum of CO_2 scaled to absolute cross sections (same as in Fig. 7) and theoretical predictions; the XPS shake-up positions (Ref. 59) are indicated; the shaded areas are due to multielectron processes, see Table I and text.

TABLE I. NEXAFS parameters of CO and CO_2.

	Carbon K edge				Oxygen K edge			
Molecule	Peak	This[a] work	Kay *et al.*[b]	Assignment	Peak	This[a] work	Barrus *et al.*[c]	Assignment
CO	1	287.3	287.5	π^*	1	533.1	534.2	π^*
	2	292.8	293.0	$3s, 3p$	2	541.1	539.1 540.4	$3s, 3p$
	3	295.1	294.7	$4p$	IP	542.1	541.7	∞
	IP[d]	296.2	295.9	∞	3	545.9		shake-up
	4	301.1	298.9	shake-up	4	550.5	550.6	σ^* shape resonance
	5	306.6	304.5	σ^* shape resonance				
	Peak	This work	Wight and Brion[e]	Assignment	Peak	This work	Wight and Brion[d]	Barrus *et al.*[c]	Assignment
CO_2	1	290.7	290.7	π^*	1,2	535.0	535.4	535.3	π^*
	2	292.7	292.7	$3s$	3	539.3	538.7	539.1 539.1	$3s, 3p$
	3	295.0	294.5	$3p$	IP	541.3	540.8	541.1	∞
	4	297.0	296.3	$4s, 4p$	4	542.5	541.9	541.5	σ^* shape resonances
	IP	297.6	297.5	∞	5	554.2	553	554	shake-up
	5	300.5	301	shake-up	6	559.9	558	558.7	σ^* shape resonance
	6	304.2	303.6	shake-up					
	7	312.2	311	shake-up					
	8	313.8	314	σ^* shape resonance					

[a]Relative peak positions near C K edge are accurate to about 0.2 eV, and to about 0.4 eV elsewhere.
[b]Reference 45.
[c]Reference 43.
[d]IP values are from Ref. 65.
[e]Reference 42.

siderations alone. In the case of CO, for example, the ground-state electronic configuration is

$$1\sigma^2 2\sigma^2 3\sigma^2 4\sigma^2 1\pi^4 5\sigma^2 2\pi 6\sigma,\ ^1\Sigma^+ ,$$

where 2π and 6σ are the unoccupied MO's. The π^* and σ^* resonance features at both the C and O edge can be immediately assigned to $1s$-2π and $1s$-6σ transitions, respectively. Similarly, the ground state of CO_2 is

$$1\sigma_g^2 1\sigma_u^2 2\sigma_g^2 3\sigma_g^2 2\sigma_u^2 4\sigma_g^2 3\sigma_u^2 1\pi_u^4 1\pi_g^4 2\pi_u 5\sigma_g 4\sigma_u,\ ^1\Sigma_g^+ ,$$

where $2\pi_u$, $5\sigma_g$, and $4\sigma_u$ are unoccupied. By using the same dipole selection rules, we can predict one π^* and two σ^* transitions from $1\sigma_g$(O $1s$)-$2\pi_u(\pi^*)$, $1\sigma_u$(O $1s$)$-5\sigma_g(\sigma^*)$, and $1\sigma_g$-$4\sigma_u(\sigma^*)$, respectively, at the O edge, and one each of π^* and σ^* transition from $2\sigma_g$(C $1s$)-$2\pi_u(\pi^*)$ and $2\sigma_g - 4\sigma_u(\sigma^*)$, respectively, at the C edge. It is apparent from this analysis and Fig. 7 that a simple MO picture can account for the number and the symmetry of the resonances observed. Quantitative analysis of these data requires the assistance of theoretical calculation and selected partial yield measurements.

Two theoretical models so far have met with reasonable success in predicting the energy positions of all the main peaks and the shape of the molecular shape resonances above the ionization threshold in small molecules. One of these approaches invokes the trapping of the photoelectron by a potential barrier,[28,29,47] the other relates the shape resonances to unoccupied (virtual) molecular orbitals.[30,31,45,48–52] The method of calculation in the former involves the use of the multiple-scattering $X\alpha$ (MS-$X\alpha$) technique extended to include continuum states, and in the latter the use of Stieltjes-Tchebycheff moment theory (STMT).

The real difference between the two descriptions is more technical than physical. Both predict the same resonance features in the photoabsorption spectra. At the resonant photon energy (for electron kinetic energy), the wave function of the photoelectron experiences an enhanced overlap with a continuum channel. In molecular-orbital theory, it is important to realize that the wave functions are confined to a linear combination of atomic orbital–molecular-orbital (LCAO-MO) picture. The interpretation of the resonant continuum orbital resembles that of an antibonding orbital, which is governed by a large contribution of the antibonding orbital in the continuum wave function. By contrast, the MS-$X\alpha$ method is based on electron scattering by the molecular potential. The electron wave function is con-

structed from a superposition of outgoing and incoming plane waves. As molecular wave functions possess nodal structures (i.e., nodes in their radial and angular parts), these nodal structures can be generated in multiple scattering theory by constructive and destructive interference between the outgoing (forward scattering) and incoming (background) waves.[53] Moreover, it is not necessary to introduce the concept of centrifugal or effective potential barrier in order to understand the resonance process.[54] Natoli has argued[55] that it is not possible to have a potential barrier in molecules as suggested by Dehmer. Nevertheless one can naively (or conveniently) picture that the presence of a potential tends to localize the wave function. Mathematically, what happens is that a potential in the Schrödinger equation contributes a node to the wave function and prohibits electrons from passing through a certain region of space. There is "no" clear distinction between the description of the bound states versus the continuum states. Below the vacuum level, in the unoccupied space, there are discrete Rydberg-type orbital which converge to continuum wave functions. In addition, there will be some localized antibonding orbital distributed throughout the Rydberg orbital. The mixing of these orbitals is governed by the energy and the symmetry of the orbital. A better description has been given by Keller and Lefebre-Brion.[56] As demonstrated by Robin[57] in cyclopropane, the f-type Rydberg orbitals are higher in energy than the C-C σ orbital and therefore do not mix with it and transition to the antibonding orbital results in a "giant resonance". A general rule of thumb is that the mixing of the localized antibonding orbital with the more diffused Rydberg orbital will redistribute the oscillator strength among all the possible combinations and the bonding-antibonding transition is ill defined and possibly spreads out in several excitations. This is actually the original idea of Mulliken who argued that one should not observed the antibonding orbital in methane.[58] Finally, it is important to realize in principle that, just like the occupied Hartree-Fock molecular orbital, the concept of antibonding orbital is the consequence of molecular-orbital theory, i.e., it is from a solution of the Schrödinger equation using a LCAO-MO formalism.

The theoretical predictions shown in Fig. 7 are those of MS-$X\alpha$ (Ref. 47) and STMT (Refs. 46 and 48) calculations. They are in good agreement with the data except the shaded peaks which are not predicted by these one-electron theories. Similar agreement has been obtained by Truesdale *et al.* who compare the single channel C 1s photoelectron yield with these theories.[4] Our absorption data are in excellent agreement with the photoelectron data of Truesdale *et al.* (except the shaded areas). In Fig. 8 we compare our data with theory in a manner similar to Truesdale *et al.*[4] where we also use a more recent calculation by Daasch *et al.*[50] who predicted the presence of two shape resonances above the threshold by using an improved STMT method.

We are particularly interested in CO_2 in that it is an excellent example for the observation of the focussing effect in EXAFS.[7,11] It has been noted in EXAFS experiments that when the absorber, the nearest-neighboring scatterer, and a second-nearest scatterer are in a linear arrangement, the single-particle, single-scattering, plane-wave approximation analysis does not yield the correct structural and dynamic parameters.[11] This is because the forward scattering as well as the backscattering by the second scatterer is enhanced by the intervening atom. We look for similar effects in the NEXAFS of oxygen where multiple scattering dominates because of the low kinetic energy of the photoelectron. In connection with this study, we have carried out a MS-$X\alpha$ calculation of the absorption of CO_2 at both the carbon and oxygen K edges. The results correctly predict the presence (within 3 eV) of all the observed shape resonances but the predicted intensity is several times too high.

We now discuss the shaded areas in Figs. 7 and 8. These are assigned to shake-up (or double-ionization) peaks. Some of these have been assigned previously.[4] We use the following criteria to assign these peaks: (a) The peak is not predicted by single-particle theory such as those shown in the figures. (b) The peak is not observed in the partial ionization cross section (for example, the single-channel 1s photoelectron yield for carbon and oxygen such as the results of Truesdale *et al.*[4]). (c) The intensity of the peak changes in other partial yield techniques. In fragmentation-yield (selected ion yield) measurements of CO, for example,[1] the shake-up final state (double excitation) which has an extra valence hole in addition to the core hole often favors the formation of ion fragments and multiply charged ions.[1,45] It is found that in the photofragmentation study of CO at the C K edge,[1,6] the peak at 301.1 eV is enhanced in the ion fragment and doubly charged ion yield because the doubly excited state can decay into the same final-state channels as those of the 1s-π^* transition leading to extensive fragmentation of the molecule.[1,6] A schematic of this process is illustrated in Fig. 9. From these discussions, we can assign the 301.1-eV peak of CO to a shake-up peak (double excitation because the energy is too low for ionization shake-up) because it is neither predicted by the theory, nor observed in the photoelectron-yield spectrum, and

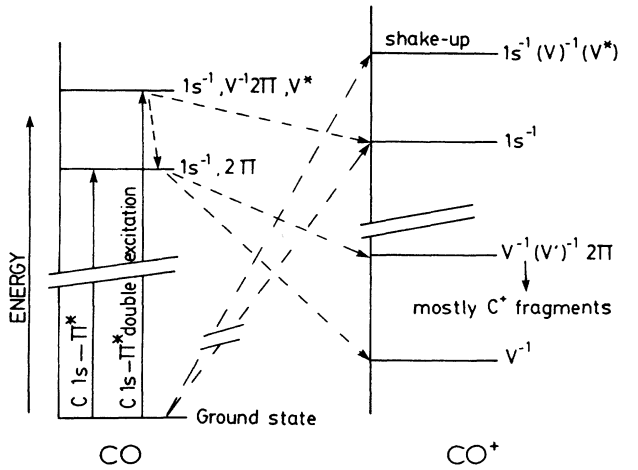

FIG. 9. Schematic energy diagram for CO and CO^+, the $1s^{-1}\,V^{-1},(V')^{-1},2\pi$ state has been shown to fragment predominantly to yield C^+ and O^+.

has an enhanced intensity in the partial ion-yield spectra. This assignment is in agreement with that of Ungier and Thomas.[44] We also note that when both shake-up and shape-resonance peaks are present in the spectrum such as in CO (Fig. 7), the shake-up peak(s) is often narrower and considerably weaker than that of the shape resonance. We assign the shaded peaks in the CO_2 spectra to shake-up transitions using similar procedures although no sufficient ion-yield data is available. However the results of Truesdale *et al.*[4] together with the calculation of Daasch *et al.*[50] and our MS-$X\alpha$ calculation strongly support that the first resonance above the O K edge in CO_2 is not a shake-up but a shape resonance. The first two shaded peaks in the C spectrum are assigned to double excitation and the remaining one is assigned to ionization shake-up based on former x-ray photoelectron (XPS) experiments.[59] The results of these analysis are summarized in Table I.

The carbon and oxygen K-edge spectra of OCS are shown in Fig. 10, together with the C 1s photoelectron-yield result of Truesdale *et al.*[4] and the EELS results of Wight and Brion.[60] It can be immediately seen from these figures that the data of Truesdale *et al.* are similar to ours but we both differ markedly from the EELS results[60] in which no apparent shape resonance is observed above both the C and the O K-edge threshold. Hitchcock *et al.*[61] have recently reinvestigated this molecule with EELS and found that there are indeed weak but clearly noticeable features in the 304- to 324-eV region. The peak positions of their spectra are in qualitative accord with the photon results, but the magnitudes remain quite different. A close examination reveals that the two prominent shape resonances observed in the photoelectron cross-section study at the C K edge[4] are seen in our data but several additional features are also observed at both

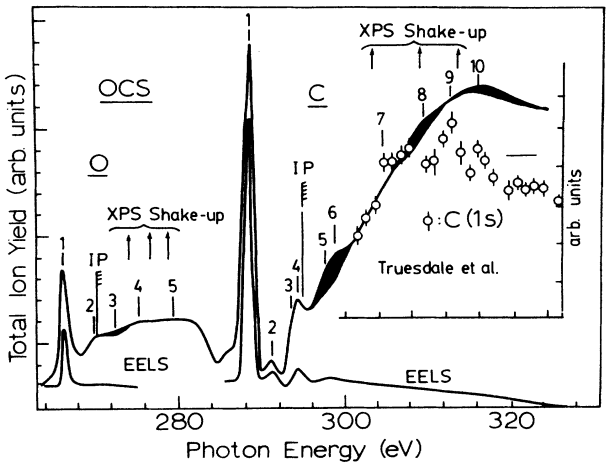

FIG. 10. Carbon and oxygen NEXAFS of OCS together with previous EELS (Ref. 60) and photoelectron data (Ref. 4), the XPS shake-up peaks are also shown for comparison, the shaded areas are assigned to shake-ups, see Table II and text for assignment.

C and O edges. We can rationalize the difference between our observation and those of Truesdale *et al.*[4] by attributing the additional features to shake-up (the XPS energy positions of the shake-up peaks[59] are marked in Fig. 10 with arrows for comparison), since these features are not detected in a single-channel measurement. At the present time we cannot offer an satisfactory explanation for the discrepancy between the photon and the EELS results. On the other hand, if the photoelectron yield spectrum (Truesdale *et al.*) is shifted by about 3 eV, the two sets of data are in reasonable agreement, without the introduction of shake-up peaks.

The ground-state configuration of OCS is

TABLE II. NEXAFS parameters of OCS.

	Carbon K edge Peak position (eV)				Oxygen K edge Peak position (eV)			
Peak	This[a] work	Wight and Brion	Truesdale *et al.*[b]	Assignment	Peak	This work	Wight and Brion[c]	Assignment
1	288.4	288.2	288	π^*	1	533.1	533.7	π^*
2	291.4	291.0 291.5		$3s,3p$	2	539.6		ns,np, shake-up
3	293.5	293.7		ns,np	IP	540.3	540.3	∞
4	294.4	294.4			3	545.3	545.3	shake-up
IP	295.2			∞				
5	297.0	297.5		shake-up	4	550.2		σ^* shape resonance
6	299.1	298.3		shake-up	5	558		σ^* shape resonance
7	~305		305	σ^* shape resonance				
8	~309			shake-up				
9	~312		312	σ^* shape resonance				
10	~315			shake-up				

[a]Uncertainty in peak positions is the same as in Table I.
[b]Reference 4.
[c]Reference 62.

TABLE III. NEXAFS parameters of $(CH_3)_2CO$.

Peak	Peak position (eV) This[a] work	Hitchcock and Brion[b]	Assignment	Peak	Peak position (eV) This work	Hitchcock and Brion	Assignment
1	287.1	286.81	$\pi^*(=CO)$	1	530.4	531.3	π^*
2	288.8	288.37	$3s, 3p(CH_3)$	2	536.0	535.7	Rydberg
		289.08	$3s, 3p(=CO)$			537.6	
		290.53	$4p(CH_3)$				
IP (CH_3)	291.2	291.1	∞	IP	537.9	537.9	∞
		291.4					
		291.9	Rydberg	3	543.7	542.8	$\sigma^*(CH_3)$
3	293.5	292.6	$\sigma^*(CH_3)$				
IP $(=CO)$	293.9	293.9	∞	4	545.1	545.3	$\sigma^*(=CO)$
4	296.7	296.8	$\sigma^*(CH_3)2CO$				
5	303.6	301.7	$\sigma^*(=CO)$				
6	~317		multiple				
7	~351		scattering				

[a]Uncertainty in peak positions is the same as in Table I.
[b]Reference 63.

$1\sigma^2 2\sigma^2 3\sigma^2 4\sigma^2 5\sigma^2 1\pi^4 6\sigma^2 7\sigma^2 8\sigma^2 9\sigma^2 2\pi^4 3\pi^4 4\pi^* 10\sigma^* 11\sigma^*, {}^1\Sigma^+$.

Transitions from 2σ(O 1s) and 3σ(C 1s) to the unoccupied orbital $4\pi^*$, $10\sigma^*$, and $11\sigma^*$ are allowed based on a simple MO picture. We can then predict the observation of one π^* and two σ^* resonances at both the C and the O edge. The two σ^* resonance peaks correspond to the $l=3,4$ partial wave channels which have been predicted by Grimm[52] and observed in the photoelectron-yield data (so called f and g resonances, respectively). Following their results, we assign two peaks at each edge to be the shape resonance (Table II), and the rest of the structure (shaded peaks) are assigned to double-excitation and shake-up peaks based on XPS data.[59] The results and assignments are summarized in Table II.

B. NEXAFS of acetone

The ionization yield spectra of $(CH_3)_2CO$ are shown in Fig. 11 together with previous EELS measurements of Hitchcock and Brion[62] and our MS-$X\alpha$ calculation of the absorption spectrum of acetone on both the carbon and oxygen edges. It can be seen from Fig. 11 that qualitatively both experimental measurements agree very well except for their intensities, i.e., resonances above the carbon K edge are more intense in the x-ray measurements. The lowest unoccupied orbital (LUMO) in acetone is a π^* orbital residing primarily at the carbyonl carbon and oxygen sites. It is expected that an intense 1s-π^* transition from the carbonyl carbon and the oxygen site would be observed. There are also σ^*-type MO's above the π^* resulting from the interaction of the carbon in carbonyl with CH_3 and with oxygen. We here confirm some of the previous assignments and reassign some features with the assistance of our MS-$X\alpha$ calculation.

The NEXAFS parameters are summarized in Table III. We note that the carbonyl carbon 1s-π^* transition (peak 1) can be confirmed from the fragmentation study[1,6] in which this transition gives rise to a very large C^+ and O^+ yield while the second narrow peak and the shoulder (peak 2) due to Rydberg transitions originating from the methyl carbon yield no such pattern. There appear to be at least two broad resonances above the ionization threshold of both carbons in the C K-edge spectrum.

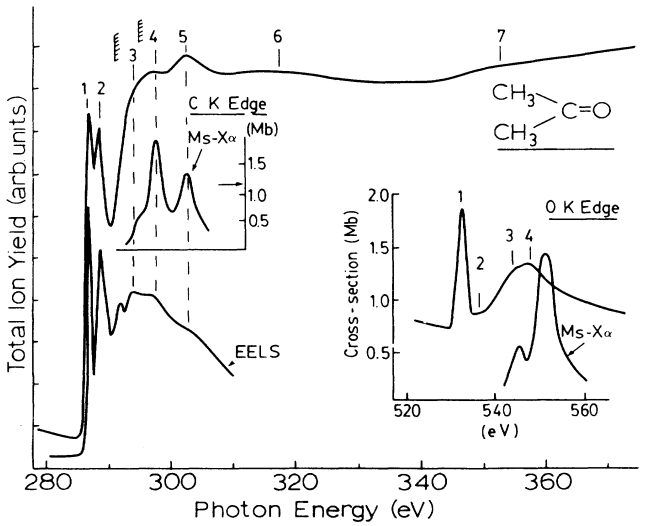

FIG. 11. Carbon and oxygen K-edge NEXAFS of acetone compared with MS-$X\alpha$ calculation (this work) and with previous EELS results, the calculated carbon edge spectrum has been shifted to lower energy by 2 eV to match the experiment, no shift is applied to the O edge results. See Table III for assignment.

Peak 5 (303.6 eV) is assigned to a σ^* shape resonance originating from the carbonyl carbon in agreement with the previous assignment.[62] It is interesting to note that the EELS measurement of this peak appears at a lower energy (301.7 eV). This discrepancy in the energy position of resonances between photon (x-ray) and pseudophoton (EELS) absorption spectrum has been observed in a number of cases,[4,35] particularly for resonances at energies far above the threshold. Although experimental uncertainty and different data-analysis procedures may contribute to the discrepancy, it is not clear whether or not the difference is fundamental. Very little is known about this problem. The peak at 296.7 eV was originally assigned to a methyl carbon $1s-CH_3$-C σ^* shape resonance[62] and was later reassigned to carbonyl carbon $1s-CH_3$-C σ^* shape resonance.[32] In the later assignment the broad peak at the carbonyl carbon threshold (293.5 eV) was also assigned to a shape resonance originating from the methyl carbon on the basis of the shape-resonance–bond-length correlation (Table III).

MS-$X\alpha$ calculation for acetone (Fig. 11) unambiguously shows three resonances above the carbon K edge. Although the absolute energies of the calculated peaks are slightly higher than observed, the energy separation and relative intensity of these peaks are in reasonable agreement with experimental observation. Thus the calculation supports the assignment of these peaks as shape resonances. It is interesting to note that the fragmentation yield spectrum of acetone[1,6] should be useful to the proper assignment of these resonances. We note in their data that the CH_3^+ yield follows the general pattern of the ionization spectrum above the threshold while the relative intensity of H^+ and CH_3CO^+ yield decreases at 293.5 eV (or increases at 296.7 and 303.6 eV). More experiments (such as Auger and ion-fragment-yield measurements) are needed to understand the relationship between fragmentation and local excitation. The oxygen K-edge NEXAFS is relatively simple. The sharp resonance below the threshold can be unambiguously assigned to the O $1s$-π^* transition. The weak Rydberg peaks observed previously were not resolved here but two broad features are observed above the threshold. The lower energy peak was previously assigned to a shake-up and the higher energy one to shape resonance.[62] Our calculation clearly predicts the presence of two resonances and we reassign the shake-up peak to another shape resonance.

C. NEXAFS of ethanol and ether molecules

Shown in Figs. 12 and 13 are the ionization yield NEXAFS of these compounds. Since some of these results have not been reported before, we marked the resonance positions on the spectrum and summarize their assignments in Table IV. Our assignments are based primarily on the work of Wight and Brion.[63] We differ in that we assign the broad peak in the vicinity of the threshold at both edges to a σ^* shape resonance, in agreement with Hitchcock *et al.*[32] and Sette *et al.*[33] Aside from the molecular-orbital picture which supports the presence of one or more σ^*-type MO's above the highest occupied molecular orbital (HOMO), we also note from the EELS

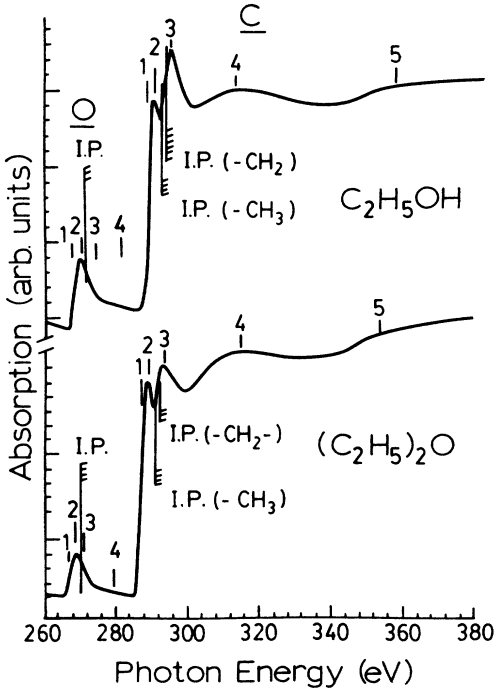

FIG. 12. NEXAFS of ethanol and diethylether (see Table IV).

data[63] and the analysis of Hitchcock *et al.*[32] that under favorable conditions the presence of the shape resonance can be confirmed experimentally. Let us consider the additivity model of absorption cross sections for the moment and compare the carbon K-edge absorption spectrum of CH_3OH with CH_4. Since oxygen only contrib-

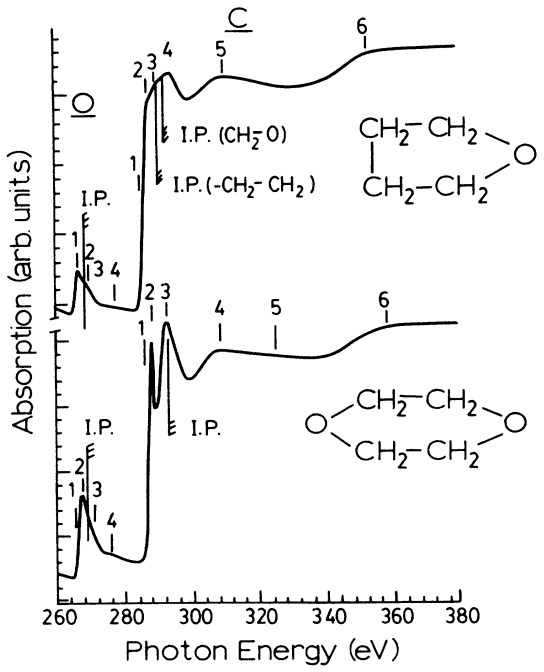

FIG. 13. NEXAFS of THF and p-dioxane, the EELS spectrum of THF has been previously reported in Ref. 78 (see Table IV).

TABLE IV. NEXAFS of C_2H_5OH, $(C_2H_5)_2O$, C_4H_8O, and $C_4H_8O_2$. (Uncertainty in peak positions is the same as in Table I. MS = multiple scattering, R = Rydberg, IP values are from Ref. 65.)

	Carbon K edge			Oxygen K edge		
Molecule	Peak	Energy (eV)	Assignment	Peak	Energy (eV)	Assignment
C_2H_5OH	1	286.9	$R(3s,3p)$	1	532.6	Rydberg
	2	288.9	$R(3s,3p)$	2	536.4	σ^*(C—O)
	IP (CH_2)	291.1	∞	IP	538.6	∞
	IP (CH_3)	292.5	∞	3	543.7	shake-up
	3	293.0	σ^*(C—O)	4	557.8	MS
	4	311.1	MS			
	5	354	MS			
$(C_2H_5)_2O$	1	286.5	$R(3s,3p)$	1	534.8	Rydberg
	2	287.9	$R(3s,3p)$			
	IP (CH_2)	291.2	∞	2	535.6	σ^*
	IP (CH_3)	292.5	∞	IP	539.3	∞
	3	293.0	σ^*	3	541.6	MS
	4	313	MS	4	557.7	MS
	5	353	MS			
C_4H_8O	1	286.9	R(C—O)	1	535.6	σ^*(O—C)
	2	289.9	R(C—C)	IP	539.3	∞
	3	291.2	σ^*(C—O)	2	540.1	σ^*(O—C)
	IP (C—C)	290.8	∞	3	543.7	shake-up or σ(O—C)
	IP (C—O)	292.5	∞	4	556.8	MS
	4	295.0	σ^*(C—C)			
	5	311.1	MS			
	6	354	MS			
p-$C_4H_8O_2$	1	286.9	R	1	533.6	R
	2	288.9	R			
	3	293.5	σ^*(C—O)	2	536.6	σ^*
	IP	293.9	∞	IP	539.3	∞
	4	309.1	σ^*(C—C)	3	542.5	shake-up
	5	325	MS	4	553.8	MS
	6	356	MS			

utes to the baseline at the carbon K edge, the edge jump for both molecules should be the same. In chemical terms CH_3OH can be regarded as CH_4 with one H being replaced by an OH group and the bonding between the methyl carbon and the hydroxyl oxygen is the only difference. Thus any change in the NEXAFS must arise from this interaction. From the data of Wight and Brion (Fig. 14), we can clearly see a broad peak near the threshold in the CH_3OH spectrum, which is absent in the CH_4 spectrum. The difference in absorption in this region is very large and the most reasonable explanation for this additional cross section is to attribute it to a carbon $1s$-σ^* shape resonance of which the final state is trapped by the molecular potential. Similar procedure can be used to identify the shape resonance at the oxygen K edge by comparing the absorption spectrum of H_2O and CH_3OH. In this case, the carbon absorption would only contribute to the base line of the O K-edge spectrum and any additional cross section in the near-edge region must arise from the bonding between O and C. We find that a corresponding shape resonance does exist at the oxygen K edge for CH_3OH. Thus this analysis together with MO calculations strongly supports the presence of a σ^* resonance. Although the maximum of the peak appears to be slightly below the ionization threshold, it still has considerable intensity at energies above the threshold. In addition, since we are dealing with a transition process, it is irrelevant whether the final state is above the threshold or not. In fact, more often than not the virtual MO's are above the vacuum level in the ground state[64] and drop down to below the vacuum level upon dipole transition due to electron–core-hole interaction. Furthermore, if we want to consider the NEXAFS on the basis of a

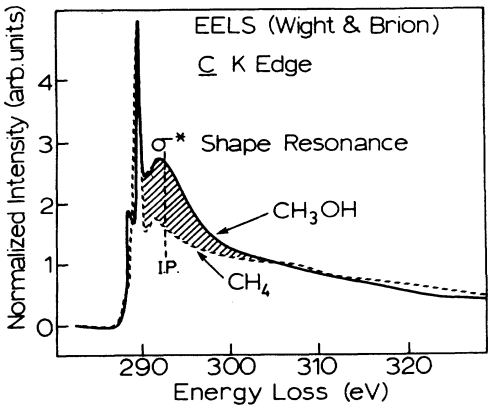

FIG. 14. Comparison of the normalized C K-edge NEXAFS of CH_4 with CH_3OH from Wight and Brion (Ref. 63). The CH_4 spectrum has been shifted to higher energy by 1.6 eV to line up the IP's.

multiple-scattering formalism,[53] the so called reference (zero) level is not the vacuum level. We return to this discussion in Sec. IV.

Returning to Figs. 12 and 13, we can confidently assign the broad and intense peak near the threshold to a shape resonance on the basis of the CH_3OH data and their assignment. Although there are supposed to be two sets of spectra arising from each carbon in the compound in connection with carbon-carbon and carbon-oxygen bonding, they are not resolved in the spectrum. Thus the energy quoted in the table is the convoluted value. The oxygen edge shape resonance can be assigned without difficulty. The assignment of other peaks are tentative at present. More quantitative assignment awaits calculation and additional yield experiments. We can see from these figures that all the carbon spectra are remarkably similar with one relatively narrow Rydberg peak and an intense shape-resonance peak near the threshold except in the case of THF where the two carbon sites are apparently different enough to show two sets of Rydberg and shape resonance transitions. The oxygen spectrum appears to be more sensitive. The overall chemical systematics are discussed in Sec. IV. We note that there are appreciable oscillations in the absorption coefficient above the carbon K edge beyond the usual NEXAFS region in contrast to similar measurements at the O K edge.[11] We attribute them to multiple-scattering resonance (oxygen is a better backscatterer than carbon).

IV. CHEMICAL SYSTEMATICS OF NEXAFS PARAMETERS

We now examine the chemical systematics of the above described observations. The data of relevance to this discussion are the position of the π^* resonance, the intensity of the π^* resonance (normalized to the absorption threshold), the ionization potential [x-ray photoelectron (XPS) binding energy values are used here], and the position and relative intensity of the shape resonances. These transitions are directly connected to orbitals that are involved in bonding. Rydberg orbitals are atomiclike and they are supported by the asymptotic wing of the Coulombic potential (outer-well states). Hence they are less chemically sensitive. A collection of relevant data is presented in Table V. Before we begin the discussion, it should be noted that the well-documented parameter in related studies is the XPS binding energy[65] [or ionization potential (IP) in the context of the discussion] which

TABLE V. Comparison of effective electron-hole interaction—final energy $U-E(f)$ at the carbon and oxygen edge.

	Carbon K edge							
Molecule[a]	π^*	$\Delta E(\pi^*)$	E_{IP}[b]	σ^*	EELS	$\Delta E(\sigma^*)$	R	$\Delta E(R)$
CO	287.3	−8.9	296.2	306.6	303.9	10.4	292.8	−3.4
CO_2	290.7	−6.9	297.6	313.8	314.0	16.2	295.0	−2.6
OCS	288.4	−6.8	295.2	305		9.8	291.4	−3.8
				312		16.8		
$(CH_3)_2\underline{C}O$	287.1	−6.8	293.9	297.6	296.4	2.8		
				303.6	301.7	9.7		
$(\underline{C}H_3)_2CO$			291.2	293.5	293.3	2.3	288.7	−2.4
$\underline{C}H_3CH_2OH$			291.1	293.0		1.9	288.9	−2.9
$CH_3\underline{C}H_2OH$			292.5	293.0		0.5		
$(\underline{C}H_3CH_2)_2O$			291.2	293.0		0.8	287.9	−4.7
$(CH_3\underline{C}H_2)_2O$			293.9	293.0		−0.9		
$(CH_2)_4O$[c]			290.8[d]	295.0[d]		4.5	289.9	−0.9
			292.5[e]	291.2[e]		−1.5	286.9	−5.6
$(CH_2)_4O_2$[c]			293.9	293.5		−0.4	288.9	−3.7
CO	533.1	−9.0	542.1	550.5	550.9	8.4	541.1	−1.0
CO_2	534.5	−6.8	541.3	542.5		1.2	539.3	−2.0
				559.9	558	18.6		
OCS	532.8	−7.5	540.3	550.2		9.9	539.6	−0.7
				558		17.7		
$(CH_3)_2CO$	530.4	−8.9	539.3	543.7	542.8	4.4		
				545.1	545.3	5.8		
C_2H_5OH			538.6	536.4		−2.2	532.6	−6.0
$(C_2H_5)_2O$			539.3	535.6		−3.7	534.7	−4.5
C_4H_8O			539.3	535.6		−3.7	534.7	−4.6
$C_4H_8O_2$			539.3	536.6		−2.7	533.6	−5.7

[a]Underscore shows the location of the core hole in the final states.
[b]XPS measurements for p-dioxine are not available. We used the value for ethyl ether instead.
[c]These compounds are cyclic molecules in which the oxygen atoms bridge two —CH_2— groups.
[d]Carbon bonded to one oxygen and one carbon.
[e]Carbon bonded to two carbons.

probes the core state by removing the electron to a final state in the continuum well above the ionization threshold. Thus chemical trend in XPS measurements is expected and has been observed universally in organic molecules on the basis of saturation and electronegativity considerations. This trend is seen from the IP values of the compounds studied (Table V). The NEXAFS parameters such as the transition energies do not necessarily follow the trend because the final state differs from molecule to molecule and, more importantly, the electron-hole interaction (arising from the Coulombic interaction of the excited electron with the core hole). This interaction, which is unimportant in XPS, plays an important role.[64] A consequence of this is the dropping down of the unoccupied orbital to below the vacuum level.

The chemical systematics of the electron-hole interaction can be discussed in terms of a simple parametrization of energies within the framework of molecular-orbital theory. Let us consider a neutral molecule at the ground state. A certain amount of energy, $-E(1s)$, is required to produce a $1s$ core hole in the molecule and a free electron. Its value is the $1s$ ionization potential (IP) obtained from XPS binding energy.[62] On the other hand, the energy of unoccupied or virtual molecular orbitals $E(\mathrm{O}^*)$ is determined by the interaction of the electron with the neutral molecule and can be measured by inverse photoemission and/or resonant electron scattering.[66–70] It has been generally recognized that the transition energy in photoabsorption should be the difference between the levels measured with inverse photoemission and photoemission lowered by an electron-hole interaction [$U(1s,2\pi^*)$ for $1s$-π^* transition, for example, or the lack of $2\pi^*$, $1s$ electron repulsion]. In practice, however, little data is available due to experimental difficulties. Thus the x-ray energy $E(\mathrm{ex})$ used to excite an $1s$ electron to the unoccupied orbital (O^*) does not equal to the difference of the absolute values of $E(\mathrm{O}^*)$ and $E(1s)$. Their differences $U(1s\mathrm{O}^*)$ is attributed to the electron-hole interaction (Fig. 15) and core-hole relaxation,

$$U(1s,\mathrm{O}^*)=-E(1s)+E(\mathrm{O}^*)-E(\mathrm{ex}) . \quad (1)$$

Although the values of most $E(\mathrm{O}^*)$ of our molecules are not known experimentally, we can still discuss the chemical implications in terms of the difference of $E(\mathrm{O}^*)$ and $U(1s,\mathrm{O}^*)$, that is,

$$\Delta E(\mathrm{O}^*)=E(\mathrm{O}^*)-U(1s,\mathrm{O}^*)=E(\mathrm{ex})-E_{\mathrm{I.P.}} . \quad (2)$$

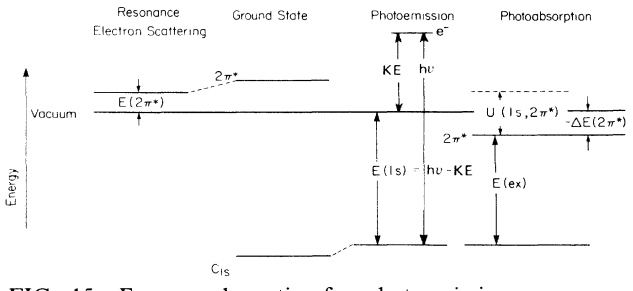

FIG. 15. Energy schematics for photoemission, resonance electron scattering, and photoabsorption of the π^* transition in CO (following Ref. 64). KE represents the kinetic energy.

In Table V, the $\Delta E(\mathrm{O}^*)$s for π^*, σ^*, and Rydberg $(3s,3p)$ states are listed as $\Delta E(\pi^*)$, $\Delta E(\sigma^*)$, and $\Delta E(R)$, respectively. The implication of these parameters to the chemical bonding in molecules is discussed below for saturated and unsaturated bonding situations.

A. Final-state electron–core-hole interaction in unsaturated molecules CO, CO_2, OCS, and $(CH_3)_2CO$: $1s$-to-π^* transitions

We first consider the carbon $1s$-π^* transition. The π^* is the lowest-unoccupied molecular orbital and its presence is common to all unsaturated molecules. For the diatomic molecule $E(\pi^*)=1.5$ eV is known from resonance electron-scattering experiments.[67] Using this value, we calculate a value of 10.4 eV for $U(\mathrm{C}\ 1s,2\pi^*)$ from Eq. (1). This value is in excellent agreement with previous results.[66] The polyatomic molecules have nearly identical $\Delta\pi^*$ values which are less negative than the CO value by 2 eV. This is somewhat surprising since the carbon-oxygen bond length in CO is much shorter than that in the rest and the term value of the antibonding π^* orbital in CO is expected to be higher than in other molecules. Thus the difference between diatomic and polyatomic molecules can only be due to a smaller U term in polyatomic molecules, where the electron in the π^* orbital is more delocalized than in CO, hence a weaker Coulombic interaction with the core.

The $\Delta E(\pi^*)$ values for the oxygen K edge $1s$-π^* transitions are very similar to those for the carbon K edge in the same molecules indicating that the π^* orbital is largely localized in the vicinity of both atoms and that it is indeed the final state common to both carbon and oxygen $1s$ to π^* MO transitions. A small increase in the $\Delta E(\pi^*)$ is observed from CO_2 to OCS and to $(CH_3)_2CO$. This trend may be understood in terms of the interaction of the carbonyl moiety with additional atoms and functional groups. A similar shift has been seen at the oxygen K edge of CO adsorbed on Ni(111),[64] and has been attributed to the final-state spatial properties of the $2\pi^*$ wave function (maximum charge density at the carbon site occurs upon O $1s$-π^* transition which maximizes the Ni-CO interaction). Since the electronegativity of the moiety involved is $\mathrm{O}>S>\mathrm{CH_3}$, and $\mathrm{CH_3}$ is the most electron donating group, best charge overlap is expected to occur at the carbonyl carbon site in acetone upon O $1s$-π^* transition and hence a bigger $\Delta E(\pi^*)$ value (the transition shifts to lower energy relative to the threshold).

B. Final-state electron–core-hole interaction in unsaturated molecules: $1s$-to-σ^* transitions

From Table V we see that all the σ^* states are above the threshold and the $\Delta E(\sigma^*)$ terms for these molecules vary from compound to compound unlike those of the C $1s$-π^* transition. This observation indicates that the energy as well as the spatial (hence the angular-momentum) characteristics of these quasibound states must vary considerably from compound to compound as a result of the different molecular potential.

The $1s$-σ^* transitions at the oxygen K-edge yield $\Delta E(\mathrm{O}$

$1s,\sigma$) values somewhat different from those of their carbon K-edge counterparts. For example the O $1s$-σ^* transition in CO appears at a lower energy (relative to the ionization threshold) than the C $1s$-σ^* transition while in polyatomic molecules CO_2, $(CH_3)_2CO$, and OCS, no discernible trend is found. Since the final states in these transitions are the same in the MO picture, these differences must arise from different U values and from the relaxation effect. The implication of this discrepancy is that the spatial distribution of the σ^* wave function is no longer localized in the carbonyl region as in $1s$-π^* transition but depends on the details of the molecular potential hence leading to different $\Delta E(\sigma^*)$ values for transitions from different atomic sites of the molecule to the σ^* molecular orbital.

C. Saturated molecules C_2H_5OH, $(C_2H_5)_2O$, C_4H_8O, and p-$C_4H_8O_2$

This class of molecules does not exhibit any $1s$-π^* resonance and their lowest-unoccupied molecular orbital (LUMO) is of σ^* character. Thus the electron–core-hole interaction may still bring the LUMO down to the vicinity of the vacuum level upon a $1s$-σ^* transition. The data in Table V for these molecules present a very interesting situation in which the σ^* resonance is just above the threshold at the carbon K edge but below the threshold at the oxygen K edge. This observation suggests that U(O $1s,\sigma^*$) is stronger than U(C $1s,\sigma^*$) in these molecules, since the σ^* orbital in this case is the LUMO common to both transitions. This result is consistent with what is observed in the $1s$-π^* transitions in OCS and acetone at both the C and O K edge.

D. Rydberg transitions

The selected Rydberg transitions listed in Table V are typical dipole transitions of atomic character. Thus they should be only marginally influenced by the molecular potential as observed. The increased interaction between the antibonding level with the core hole is due to the penetration of the antibonding wave function into the molecular core. A Rydberg orbital without a precursor will not be penetrating and the effect due to the formation of a core hole will be smaller. Thus the small $\Delta E(R)$ values in Table V strongly suggest that U(C $1s$, Rydberg) is very small in comparison with U(C $1s$, $2\pi^*$) of the $1s$-π^* transition. This comparison serves to illustrate the importance of the spatial characteristics of the final-state wave function. The $\Delta E(R)$ values for the Rydberg transitions at the oxygen K edge are very similar to those observed at the carbon K edge as expected. Again since the Rydberg orbitals are quite diffuse, the electron-hole interaction of the excited electron is small and relatively unimportant.

V. CORRELATION OF SHAPE RESONANCE WITH BOND LENGTHS

It has been suggested that the core-level excited molecular shape resonance observed in molecules from the threshold to 20 eV above can be correlated to the bond length between the absorbing atom and its nearest neighbor(s) in the framework of an electron-scattering formalism. Hitchcock *et al.*[32] and Stohr[70] *et al.* have studied the systematics of this correlation for a large number of small molecules in the gas phase and adsorbed on the surface and shown that an empirical correlation between the position of the σ^* shape resonance relative to the threshold and the bond length exists for pseudo-isoelectronic low-Z (atomic number) molecules. This model is based on the consideration that the low-energy photoelectron is scattered in the interatomic region of the atoms of interest. The physical details of this model have recently been challenged by Piancastelli *et al.*[34,36] We present here the correlation between bond length and the energy positions of the shape resonance observed in our data and discuss the results in terms of various views. Figure 16 shows the plot of the energy position of the σ^* versus the bond length of the atomic pair of interest. We can see that with the exception of CO_2 and OCS (which are known to be anomalous in this respect) two parallel correlations are observed for the carbon and oxygen K-edge results. This pattern is similar to that reported by Hitchcock *et al.*[32] The general rule that for chemically similar systems, the closer the shape resonance to the threshold, the longer the bond seems to hold only qualitatively. We attribute the discrepancies (e.g., between the diethylether and the alcohol results) to the notion that the σ^* orbital is not necessarily localized in the interatomic region between the atomic pairs of interest in the same manner in all molecules. As we suggested in the discussion in previous sections, σ^* being a common final state for both carbon and oxygen $1s$-σ^* transitions is only loosely defined. Since a good correlation of this sort requires the confinement of the photoelectron in the interatomic region of the bond pair in very similar manner in all the molecules studied, this correlation will break down when the spatial distribution of the σ^*-state wave function varies drastically from compound to compound. The fact that this correlation works semiquantitatively for a large number of molecules indicates that the

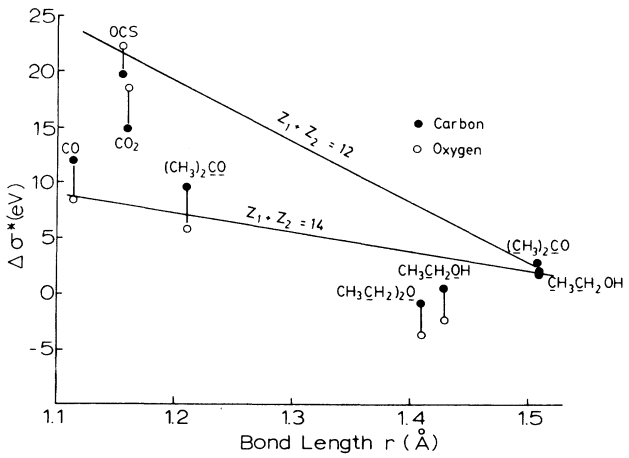

FIG. 16. σ^* shape-resonance energy position (relative to threshold) and bond-length correlation from our measurements. The correlations reported by Hitchcock *et al.* (Ref. 32) (where Z_1 and Z_2 are the atomic number of the pair) are also shown for comparison.

aforementioned requirement is generally met in most chemically similar situations. In addition, a scattering-type correlation should be r (bond length) versus k (momentum) or $\sqrt{E}$. Thus an uncertainty in the peak position of the σ^* has a much smaller effect in k, hence the bond length r.

One would like to ask whether or not the shape-resonance–interatomic-distance correlation can be applied to atomic pairs that are not "bonded" directly in these molecules. Let us consider, for example, the following pairs: the methyl carbon —CH_3 and the carbonyl oxygen C=O in acetone and the terminal carbon and hydroxyl oxygen in ethanol. It is apparent, however, from Table V and Fig. 11, that such a shape resonance can not be identified. Therefore, it is reasonable to state that unlike EXAFS this correlation does not appear to be applicable for "nonbonded" atomic pairs in these molecules. This is not unexpected since the σ^* orbital does not localize within the shortest interatomic distance of the pair of interest.

These "nonbonded" entities will, however, play an important role in the behavior of the absorption coefficient beyond the shape resonances (states that can be connected to virtual molecular orbital). In CH_3CH_2OH, for example, the C 1s photoelectron of the CH_3 group will be scattered by the CH_2 and the OH group via single or multiple pathways. These multiple scattering processes will modulate the absorption coefficient but in a different manner than EXAFS (a single-particle, single-backscattering process) would. Yet both processes would lead to oscillations in the absorption coefficient.

The carbon K-edge NEXAFS in all the saturated molecules show unusually strong oscillations in the energy region 20–100 eV above the threshold (peaks 4 and 5, and 5 and 6 in Figs. 12 and 13, respectively). This region is well beyond the region for shape resonances but the lower-energy part (peaks 4 and 5 in Fig. 12 and Fig. 13, respectively) is not quite in the usual EXAFS region yet. In Fig. 17, we show the theoretical EXAFS of ethanol using the parameters of Teo and Lee[71] and of McKale *et al.*[72] It is immediately apparent from the comparison of these results with the experimental spectrum (Fig. 12) that the conventional theory with plane-wave approximation does not account for the observation, a situation we encountered earlier in the oxygen K-edge EXAFS study.[11] The calculated EXAFS based on spherical-wave phase and amplitude[72] yields better agreement with the experiment in peak position, i.e., the position of peak 5 in the enthanol spectrum (Fig. 12). However, peak 4 in the spectrum is not accounted for in both calculations. This low-energy peak is most likely originated from multiple-scattering processes. A number of approaches has been suggested to account for the behavior of the absorption spectra of polyatomic molecules in this region, such as the multiple-scattering formalism of Benfatto *et al.*[73] or the spherical-wave formalism of EXAFS within the single-scattering framework, or perhaps a combination of both. It was pointed out recently[11] that the lack of truely core electrons and the strong molecular potential in low-Z atoms may be responsible for the apparent phase shifts. Our oxygen K-edge EXAFS[11] of the same molecules discussed here show that the discrepancy in phase shift is not a single function of interatomic distances, indicating that spherical waves alone cannot describe the experimental data satisfactorily, at least in these low-Z molecules with short bonds. The spectral patterns shown in Figs. 12 and 13 are remarkably similar for all the saturated molecules discussed here while much weaker structures are observed in CO, CO_2, and OCS. The fast oscillating behavior and large amplitude strongly suggest that longer bonds are present and multiple scattering is important. Various formalisms[73–75] have been proposed to treat these phenomena in the near-edge region. We do not attempt to treat the data according to the these formalisms in this paper.

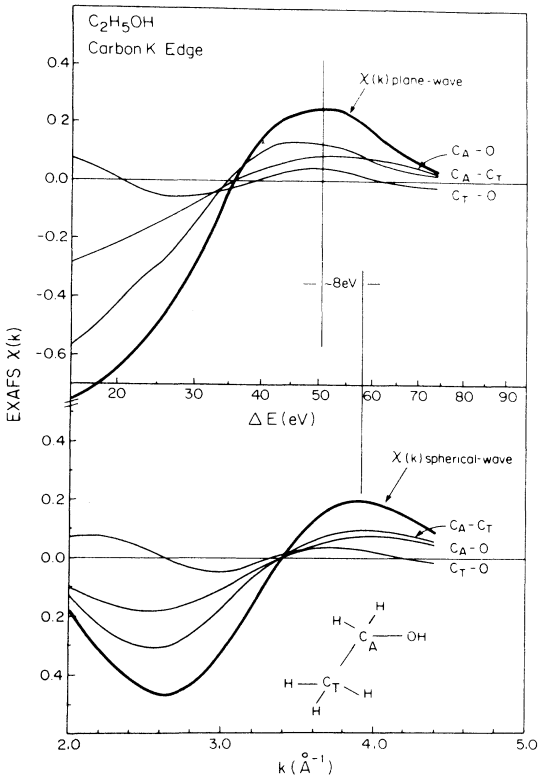

FIG. 17. The first oscillation of the EXAFS calculated for the carbon K-edge of ethanol using the phase shifts and amplitudes of Teo and Lee (Ref. 71) (plane wave) and those of Mckale *et al.* (Ref. 72) (spherical wave).

VI. ABSORPTION SPECTROSCOPY WITH LUMINESCENCE YIELD

We now return to the discussion of an alternate form of absorption spectroscopy. By-product-yield detection has been widely used in place of the direct measurement, especially in EXAFS.[11,16–26] These by-products can be divided into two groups: the primary products generated in the vicinity of the atomic core, and the secondary products generated elsewhere. The primary products include photoelectrons from single-particle and multielectron events (shake-up and shake-off), positive ions with one core hole, and possibly with additional valence holes

and excitations. It should be noted that the single-electron ionization cross section (measurements of Truesdale *et al.*[4]) is not the same as the absorption coefficient which is the sum of all partial cross sections. In addition, the total cross section is the sum of the absorption and scattering cross sections (although the latter is small in many cases of interest). Decay products generated in the cascade of the core-hole states can also be photons of energies ranging from the infrared to the x-ray region from the deexcitation of the highly disturbed electron cloud, free ions from rupturing bonds, and Auger electrons. Since the primary event cannot be isolated easily from the medium, energetic primary particles (photons, electrons, and ions) will excite surrounding medium through a series of collisions and various energy-transfer mechanisms, causing more particles to be generated which we call secondary products. Both primary and secondary processes may yield optical luminescence.

Direct product yield from a particular channel often has its own energy dependence and is not always directly proportional to the absorption cross section, particularly near the threshold. The photoelectron yield, for example, reduces to zero below the absorption edge while absorption remains finite (excitation). In EXAFS, this partial cross section is the one of interest, but it can be used only when experimental conditions allow (photoelectron diffraction complicates the detection).[76] The shake-up channel, on the other hand, peaks at energies near the absorption edge, and bears little resemblance to the single-channel spectrum.[4]

Since an ion with a core hole from a particular excitation in the near-edge region may decay in different channels, the number of particles in a particular channel depends on the branching ratio. Therefore, the yield of the direct product from a particular path is often not directly proportional to the absorption cross section. But if products of a few major channels are collected at the same time, such as the total current in a molecular-jet experiment, the yield can be a good approximation of the absorption spectrum.

Secondary products, being generated by particles of a wide energy range often lose the memory for a specific process. As a result, their yields integrated over a wide energy range, are often a good approximation of the absorption cross section, except for a smooth energy-dependent factor simply because more secondary products are generated when more photon energy is deposited in the material.

We now return to the Figs. 3, 5, and 6 and compare the optical luminescence-yield and the ionization-yield spectra with the absorption spectra. In an ion-chamber experiment, the ions collected are generated in many different decay and secondary processes. Hence the total ion yield is expected to resemble the absorption spectrum. The optical luminescence however, represents only a narrow band in the ion, atomic or molecular spectrum. With a high-resolution spectrometer, one may selectively study a particular decay product. Information about these decay products will lead to the understanding of the dynamics of core-hole states, and eventually of the absorption process itself. The use of such a technique was demonstrated recently by Yang *et al.*[14] in a study of the soft-x-ray-induced optical luminescence spectrum of O_2. They identified two emission bands coming from the O_2^+ ions (mainly secondary products) and O_2^{2+} ion (mainly decay products), respectively. The O_2^{2+} band was used to detect with great sensitivity and to identify a previous unknown shake-up state.

In our experiment, the optical emission spectra of the molecules were not investigated and only the total emission was collected. It can be seen from Figs. 5 and 6 that the unsaturated molecules exhibit a normal spectrum while the saturated molecules exhibit a drastic reduction in luminescence above the ionization threshold. Without the emission spectrum we can only suggest that above threshold less luminescent species become abundant or a luminescent species which is present below threshold becomes less abundant. It is reasonable to expect that more doubly charged particles and fragments are created above the threshold particularly for larger molecules and this may be the reason for the discrepancy. Further investigation is needed before final conclusions can be reached.

VII. SUMMARY AND CONCLUSIONS

We have reported the carbon and oxygen K-edge NEXAFS recorded with synchrotron radiation and discussed the origin of the resonances observed in connection with previous synchrotron partial cross section results, EELS results, and theoretical predictions.

Several conclusions can be drawn from these studies. (a) NEXAFS recorded with synchrotron radiation complements the EELS work in the intermediate energy region above the threshold so that shape resonance features can be more reliably identified. (b) Multielectron processes associated with absorption can be identified by using partial yield measurements (yield measurements that are favored by the shake-up process). (c) The interplay of the transition energy and spatial characteristics of the final state with the electron-core interaction determines the appearance of the NEXAFS and is chemically sensitive to the structure and bonding of the system. (d) The correlation of the bond length with the position of the shape resonance seems to hold semiquantitatively for bonding pairs indicating that the wave function of the so-called σ^* shape resonance is indeed confined in the vicinity of the bonding pair. For indirectly "bonded" pairs, however, such a correlation cannot be established. (e) Strong oscillations observed beyond the NEXAFS region in the K-edge spectrum have been analyzed in terms of the single-particle, single-scattering model. The results show, as in the case of the oxygen results reported earlier, that this model cannot reproduce the observed data. This observation suggests that in all these low-Z molecules, particularly the polyatomic ones, multiple-scattering contributions may still be important in the EXAFS region.

ACKNOWLEDGMENTS

We wish to thank Dr. A. P. Hitchcock for communicating his results prior to publication and discussion. The data presented here were recorded at the National

Synchrotron Light Source which is supported by the U.S. Department of Energy, Division of Material Science and Division of Chemical Science under Contract No. DE-AC02-76CH00016. One of us (T.K.S.) wishes to thank the Ontario Centre for Materials Research (OCMR) and the National Science and Engineering Research Council of Canada for financial support. Research at the University of British Columbia was supported by a strategic grant from the National Science and Engineering Research Council (Canada). Work at Stony Brook was supported in part by the U.S. Air Force Office of Scientific Research under Contract No. F-49620-87-K0001.

---

*Present address: Canadian Synchrotron Radiation Facility, Synchrotron Radiation Center, University of Wisconsin–Madison, Madison WI 53589.

[1]W. Eberhardt, T. K. Sham, R. Carr, S. Krummacher, M. Strongin, S. L. Weng, and D. Wesner, Phys. Rev. Lett. **50**, 1038 (1983).

[2]C. M. Truesdale, S. Southworth, P. H. Kobrin, U. Becker, D. W. Lindle, H. G. Kerlhoff, and D. A. Shirley, Phys. Rev. Lett. **50**, 1265 (1983).

[3]W. Eberhardt, J. Stohr, J. Feldhaus, E. W. Plummer, and F. Sette, Phys. Rev. Lett. **51**, 2370 (1983).

[4]C. M. Truesdale, D. W. Lindle, P. H. Kobrin, U. E. Becker, H. G. Kerkhoff, P. A. Heimann, T. A. Ferrett, and D. A. Shirley, J. Chem. Phys. **80**, 2319 (1984).

[5]K. Muller-Dethlefs, M. Sander, L. A. Chewter, and E. W. Schag, J. Phys. Chem. **88**, 6098 (1984).

[6]W. Eberhardt and T. K. Sham, Proc. SPIE **447**, 143 (1984).

[7]J. A. R. Samson, J. Opt. Soc. Am. **54**, 6 (1964); J. A. R. Samson and G. N. Haddad, *ibid.* **64**, 47 (1974).

[8]B. X. Yang, J. Kirz, and T. K. Sham, Phys. Lett. **110A**, 301 (1985); Nucl. Instrum. Methods **236**, 419 (1986).

[9]P. Morin, G. G. B. de Souza, I. Nenner, and P. Lablanquie, Phys. Rev. Lett. **56**, 131 (1986).

[10]M. C. Nelson, J. Murakami, S. L. Anderson, and D. M. Hanson, J. Chem. Phys. **86**, 4442 (1987).

[11]B. X. Yang, J. Kirz, and T. K. Sham, Phys. Rev. A **36**, 4298 (1987).

[12]B. X. Yang, J. Kirz, Y. H. Kao, and T. K. Sham, Nucl. Instrum. Methods **246**, 523 (1986).

[13]K. Tohji, D. M. Hanson, and B. X. Yang, J. Chem. Phys. **85**, 7492 (1986).

[14]B. X. Yang, D. M. Hanson, and K. Tohji, J. Chem. Phys. **89**, 1215 (1988).

[15]W. Eberhardt, Phys. Scr. **T17**, 29 (1987).

[16]See, for example, Proceedings to the IV International Conference on EXAFS and Near Edge Structure [J. Phys. (Paris) Colloq. C **8**, (1986)].

[17]P. A. Lee, P. H. Citrin, P. Eisenberger, and B. M. Kincaid, Rev. Mod. Phys. **53**, 769 (1981).

[18]J. Stohr, L. Johansson, I. Lindau, and P. Pianetta, Phys. Rev. B **20**, 664 (1979).

[19]J. Jaklevic, J. A. Kirby, M. P. Klein, A. R. Robertson, G. S. Brown, and P. Eisenberger, Solid State Commun. **23**, 679 (1977).

[20]R. Jaeger, J. Feldhaus, J. Hasse, J. Stohr, Z. Hussain, D. Menzel, and D. Norman, Phys. Rev. Lett. **45**, 1870 (1980).

[21]E. A. Stern and S. M. Heald, Rev. Sci. Instrum. **50**, 1579 (1979).

[22]T. K. Sham and S. M. Heald, J. Am. Chem. Soc. **105**, 5142 (1983); T. K. Sham and R. A. Holroyd, J. Chem. Phys. **80**, 1026 (1984).

[23]J. Goulon, P. Tola, M. Lemonnier, and J. Dexpert-Ghys, Chem. Phys. **78**, 347 (1983).

[24]G. Martens, P. Rabe, G. Tolkieln and A. Werner, Phys. Status Solidi A **55**, 105 (1979).

[25]M. E. Kordesch and R. W. Hoffman, Phys. Rev. B **31**, 6233 (1985).

[26]T. K. Sham and R. G. Carr, J. Chem. Phys. **83**, 5914 (1985).

[27]J. L. Dehmer, J. Chem. Phys. **56**, 4496 (1972).

[28]J. L. Dehmer and D. Dill, Phys. Rev. Lett. **35**, 213 (1975).

[29]J. L. Dehmer, in *Resonances in Electron-Molecular Scattering, van der Waal Complexes and Reaction Dynamics,* edited by D. G. Truhlar (American Chemical Society, Washington, D.C., 1984).

[30]D. L. Lynch, V. McKoy, and R. R. Lucches, in Ref. 29.

[31]P. W. Langhoff, in Ref. 29.

[32]A. P. Hitchcock, S. Beautieu, T. Steel, J. Stohr, and F. Sette, J. Chem. Phys. **80**, 3927 (1984).

[33]F. Sette, J. Stohr, and A. P. Hitchcock, J. Chem. Phys. **81**, 4906 (1984).

[34]M. N. Piancastelli, D. W. Lindle, T. A. Ferrett, and D. A. Shirley, J. Chem. Phys. **86**, 2765 (1987).

[35]A. P. Hitchcock and J. Stohr, J. Chem. Phys. **87**, 3253 (1987).

[36]M. N. Piancastelli, D. W. Lindle, T. A. Ferrett and D. A. Shirley, J. Chem. Phys. **87**, 3255 (1987).

[37]B. X. Yang, J. Kirz, and I. McNulty, SPIE Proc. **689**, 34 (1987).

[38]L. G. Barratt, C. F. Hempstead and E. L. Jossen, Phys. Rev. **105**, 1228 (1957).

[39]A. P. Hitchcock, P. Lablanquie, P. Morin, E. Lizon, A. Lugrin, M. Simon, P. Thiry, and I. Nenner, Phys. Rev. A **37**, 2448 (1988).

[40]R. E. Lavilla, J. Chem. Phys. **63**, 2733 (1975).

[41]G. R. Wight, C. E. Brion, and M. J. van der Wiel, J. Electron. Spectrosc. **1**, 457 (1973).

[42]G. R. Wight and C. E. Brion, J. Electron. Spectrosc. **3**, 191 (1974); **4**, 313 (1974).

[43]D. M. Barrus, R. L. Blake, A. J. Burek, K. C. Chambers, and A. L. Pregenzer, Phys. Rev. A **20**, 1045 (1979).

[44]L. Unigier and T. D. Thomas, Phys. Rev. Lett. **53**, 435 (1984).

[45]R. B. Kay, Ph. E. van der Leeuw and M. J. van der Wiel, J. Phys. B **10**, 2513 (1977).

[46]N. Padial, G. Csanak, B. V. McKoy and P. W. Langhoff, J. Chem. Phys. **69**, 2982 (1978).

[47]J. L. Dehmer and D. Dill, Argonne National Laboratory Report No. ANL-77-65, p. 65 (unpublished).

[48]N. Padial, G. Csanak, B. V. McKoy, and P. W. Langhoff, Phys. Rev. A **23**, 218 (1981).

[49]R. R. Lucchese and B. V. McKoy, Phys. Rev. A **26**, 1406 (1982).

[50]R. Daasch, E. R. Davidson, and A. U. Hazi, J. Chem. Phys. **76**, 6031 (1982).

[51]W. Thiel, J. Electron. Spectrosc. **31**, 151 (1983).

[52]F. A. Grimm, Chem. Phys. **53**, 71 (1980).

[53]*X ray Absorption, Principles, Applications, Techniques of EXAFS, SEXAFS and XANES,* edited by D. C. Kroningberger and R. Prins (Wiley, New York, 1988).
[54]M. B. Robin, *Higher Excited States of Polyatomic Molecules* (Academic, New York, 1985), Vol. III.
[55]R. Natoli, in *EXAFS and Near Edge Structures,* Vol. 27 of Springer Series on Chemical Physics (Springer, New York, 1983), p. 43.
[56]F. Keller and H. Lefebrve-Brion, Z. Phys. D **4**, 15 (1986).
[57]M. B. Robin, Chem. Phys. Lett. **119**, 33 (1985).
[58]R. S. Mulliken, Acc. Chem. Res. **9**, 7 (1976).
[59]C. J. Allen, U. Gelius, D. A. Allision, G. Johnson, H. Siegbahn, and K. Siegbahn, J. Electron. Spectrosc. **4**, 335 (1974).
[60]G. R. Wight and C. E. Brion, J. Electron. Spectrosc. **4**, 335 (1974).
[61]A. P. Hitchcock (private communication).
[62]A. P. Hitchcock and C. E. Brion, J. Electron. Spectrosc. **19**, 231 (1980).
[63]G. R. Wight and C. E. Brion, J. Electron. Spectrosc. **4**, 25 (1974).
[64]Y. Jugnet, F. J. Himpsel, Ph. Avouris, and E. E. Koch, Phys. Rev. Lett. **53**, 198 (1984).
[65]Compilation of binding energies can be found in A. A. Bakke, H. W. Chen and W. L. Jolly, J. Electron Spectrosc. **20**, 333 (1980); K. D. Bomben, C. J. Eyermann, and W. L. Jolly (unpublished).
[66]F. J. Himpsel and Th. Fanster, Phys. Rev. Lett. **49**, 1583 (1982), Th. Fauster and F. Himpsel, Phys. Rev. B **27**, 1390 (1983).
[67]H. Ehrhardt, L. Langhans, F. Linder, and H. S. Taylor, Phys. Rev. **173**, 222 (1968).
[68]G. J. Schulz, Rev. Mod. Phys. **45**, 423 (1973).
[69]K. D. Jordan and P. D. Burrow, Acc. Chem. Res. **11**, 341 (1987).
[70]J. Stohr, J. L. Gland, W. Eberhardt, D. Outka, R. J. Madix, F. Sette, R. J. Koestner, and U. Dobler, Phys. Rev. Lett. **51**, 2414 (1983).
[71]B. K. Teo and P. A. Lee, J. Am. Chem. Soc. **101**, 2815 (1979).
[72]A. G. Mckale, B. W. Veal, A. P. Paulikas, S. K. Chan, and G. S. Knapp, J. Am. Chem. Soc. **11**, 3763 (1988).
[73]M. Benfatto, C. R. Natoli, A. Bianconi, J. Garcia, A. Marcelli, M. Fanfoni, and I. Davoli, Phys. Rev. B **34**, 5774 (1987).
[74]J. B. Pendry, J. Phys. C **8**, 2413 (1975).
[75]T. Fujikawa, J. Phys. Soc. Jpn. **50**, 1321 (1981).
[76]G. M. Rothberg, K. M. Choudhary, M. L. DenBoer, G. P. Williams, M. H. Hecht, and I. Lindau, Phys. Rev. Lett. **53**, 1183 (1984).
[77]Henke *et al.*, At. Data Nucl. Data Tables **27**, 1 (1982).
[78]D. C. Newbury, I. Ishi, and A. P. Hitchcock, Can. J. Chem.